13

Simulation of polycrystalline beryllium sputtering by H, D, T atoms

© P.Yu. Babenko, V.S. Mikhailov, A.P. Shergin , A.N. Zinoviev

Ioffe Institute, St. Petersburg, Russia
e-mail: zinoviev@inprof.ioffe.ru

Received January 25, 2023
Revised February 22, 2023
Accepted March 4, 2023

The results of modeling the sputtering coefficients of polycrystalline beryllium by hydrogen isotopes in the range of collision energies of 8 eV−100 keV and their dependences on the angle of incidence of the beam on the surface are presented. This data is necessary for estimating the sputtering of the first wall in the ITER tokamak made from beryllium. A strong surface shape influence on obtained results is shown. The limiting cases of a flat potential barrier (smooth surface) and a spherical potential barrier (a surface consisting of spikes) are considered. The effect of collision cascades on the sputtering coefficient has been established. The dependences of the average depth of sputtered particle formation on the bombarding particles energy are obtained for various angles of beam incidence on the target. The energy spectra and angular dependences of the ejection of sputtered particles are calculated for different energies of bombarding beam atoms. It is shown that the presence of an attractive well in the potential of an incident particle surface changes the sputtering coefficient dependence on incidence angle at small glancing angles.

Keywords: Sputtering coefficients, energy and angular distributions of sputtered particles, interatomic potential, hydrogen isotopes, beryllium.

DOI: 10.21883/TP.2023.05.56074.12-23

Introduction

The development of environmentally friendly and renewable energy sources is among the priority studies in the Russian Federation. Controlled thermonuclear fusion is the most promising and safe source of renewable energy. At the moment, many research teams are participating in the international ITER project, designed to demonstrate the technical feasibility of obtaining thermonuclear energy. One of the main problems to be solved is the interaction of high-temperature plasma with the surface of the reactor wall. Extremely intense flows of fast atoms, ions, electrons and neutrons will take over the beryllium wall of the tokamak, as well as the tungsten divertor. In turn, the atomized particles of tungsten and beryllium trapped in the plasma can radically change the operation mode of the reactor, or even disable the plant, therefore much attention is paid to the issue of admixtures entering the reactor, in particular, these issues were considered in the studies of [1–3]. It is necessary to know the sputtering coefficients of hydrogen, deuterium and tritium particles to calculate plasma parameters, as well as for a number of experimental diagnostics of the ITER tokamak. At present, experimental data on these sputtering coefficients vary greatly, and are given only for a narrow range of parameters of sputtering particles, and there are no such data for tritium. There are quite detailed calculations of the sputtering coefficients of various materials performed in the works of the Eckstein group [4,5] within the binary approximation using the KgF potential [6].

The studies [7–12] also cover the sputtering of materials that are used in plasma units. Much attention is paid to the calculations of multiparticle interaction potentials, which are needed for modeling the sputtering coefficients [13–18].

The aim of this study is to obtain data on the coefficients of sputtering of beryllium by hydrogen isotopes for a wide range of initial energies 8 eV−100 keV based on the use of the most accurate interatomic interaction potentials, including multiparticle ones, to describe particle scattering. It also seemed important to obtain the relationships of the spray coefficients on the angle of incidence of the sputtering particle. A summary of the results obtained is provided in [17]. The contribution of the mechanism of atomization of near-surface layers by a flow of backscattered particles is proposed and discussed to describe the obtained relationships.

An important problem is also the calculation of the angular and energy characteristics of the sprayed particles. This information was obtained for the first time and is needed to calculate the penetration of atomized impurity atoms into the plasma.

1. Description of methodology

The code developed by us based on the Monte Carlo method was used for calculations. The target was a set of microcrystals the size of one elementary beryllium cell, randomly oriented in space. Thermal oscillations of target atoms were taken into account. The amplitude of the oscillations was calculated according to Debye−Waller theory, from the volume temperature of Debye 1440°K [18]

and was assumed to be 0.059 Åwhich is characteristic of beryllium at room temperature.

The calculation of the spray coefficients can be divided into two stages. The first stage: analysis of the trajectory of the incoming particle. In case of an elastic collision, the incoming particle transfers part of its energy to the target particle. All crystal particles that have received energy higher than the surface binding energy $E_s = 3.32$ eV, fall into a separate data array on recoil particles, in which their position in the crystal, their momentum and the transmitted energy are recorded. The trajectories of recoil particles from the recorded array are considered at the second stage of calculations. Particles that have flown into a vacuum outside a solid and have overcome the surface barrier 3.32 eV, are considered to be atomized. Recoil particles can also transmit the necessary momentum to other target atoms. They are also added to the array of recoil particles, which allows you to fully take into account the cascades of collisions.

The interaction of the incoming hydrogen isotope atoms with the target atoms of beryllium is described in the approximation of paired collisions. As the experience of previous work on the description of the reflection of hydrogen atoms from the surface of [19,20], the passage of the beam through thin films [21], the calculation of nuclear braking losses [22] showed that the results obtained are very sensitive to the choice of the interaction potential of the incoming particle with the target atoms. It was found that the paired potentials obtained within the framework of the density functional theory with correction of the depth of the potential well in accordance with the data of spectroscopic measurements are well aligned with the experimental data obtained during the study of scattering in the gas phase [23]. Data on the interaction potential of hydrogen atoms with beryllium were taken from the work [24–25]. The difference in masses of isotopes has almost no effect on the interaction potential, since the adjustment leads to a slight change in the reduced electron mass. This is confirmed by spectroscopic measurements showing that the parameters of the potential well for different isotopes differ slightly (see [26,27]).

The energy losses of the incoming particles and the energy of the recoil particles during elastic scattering for a given potential are calculated precisely from the conservation laws. Energy losses during braking on the target electrons were taken into account at each collision as the product of the electronic braking capacity by the length of the trajectory between collisions.

For energies below 10 keV, there is no experimental data on the inhibition of hydrogen atoms in beryllium. Reliable experimental data were used for aluminum [28], which show that in the case under consideration, at collision energies below 10 the keV model of particle braking on free electrons works well, and the braking capacity is proportional to the collision velocity. Applying scaling to the difference in electron density in beryllium and aluminum using the technique proposed in [29], we obtained the expression: if the energy of the bombarding beam is $E_0 < 10\,000$ eV, then

$$\frac{dE}{dx}\left[\frac{\text{eV}}{\text{Å}}\right] = 2.758 \cdot \left(\frac{E_0[\text{keV}]}{m_1}\right)^{0.4803}. \quad (1)$$

At energies above 10 keV, a more complex expression was used, obtained by approximating the SRIM [30] database data:

$$\frac{dE}{dx}\left[\frac{\text{eV}}{\text{Å}}\right] = 4.228 + 0.496 \cdot x - 9.91 \cdot 10^{-3} \cdot x^2 + 8.604 \cdot 10^{-5} \cdot x^3 - 2.860 \cdot 10^{-7} \cdot x^4,$$

$$x = \frac{E_0[\text{keV}]}{m_1}. \quad (2)$$

Here m_1 — the mass of the hydrogen isotope.

The parameters of multiparticle potentials obtained in [24,25] using the density functional theory were used for calculating the trajectories of recoil particles. Nuclear braking losses associated with multiple scattering on target atoms prevailed when the trajectories of recoil atoms were considered. The role of electronic braking losses in this case is small. However, we used data from the SRIM [30] database.

For the set of required statistics, we considered 10^6 incoming particles, and in the case of calculation of the threshold behavior of the sputtering coefficient, the number of incoming particles reached 10^8.

The calculation results are sensitive to the shape of the potential barrier at the solid−vacuum boundary. The surface potential can be assumed spherical for a highly uneven surface consisting of atomic-scale points, or planar for a smooth surface. In the first case, the criterion for the departure of the atomized particle consists in the requirement that the energy of the atomized particle E_b exceeds the surface bonding energy E_s, and in case of a planar potential, the condition $E_b \cdot \cos^2(\theta) > E_s$ is required, here θ is the angle of departure of the atomized particle. High surface roughness can be expected with intensive sputtering of the wall. The calculation using these limits characterizes the effect of surface roughness on the spray coefficients. The spray coefficients will have values between the two considered limiting cases for sputtering a real surface.

2. Coefficients of beryllium atomization by hydrogen isotopes at normal beam incidence on the target

Figure 1 shows the coefficients of beryllium sputtering by hydrogen isotopes depending on the energy of the impinging particles. Our calculation for a spherical barrier — lines with solid circles, lines with open circles — calculation for a planar barrier. Symbols — are experimental values of the

spray coefficient of different authors, and the dashed line — averaging of calculated data from the studies [4,5].

It can be seen from Fig. 1 that there are no experimental data for the pair H–Be and energies less than 60 eV. The values of the sputtering coefficient calculated using our program describe the experimental data better than the calculation of the Eckstein group [4,5]. There is a large experimental dataset in the case of sputtering a beryllium target with deuterium atoms. As can be seen from Fig. 1, at energies of bombarding particles of the order of 100 eV, a very large spread of values obtained from the experiment is observed. For the system T–Be, there are no experimental data on the sputtering coefficients, but since there is a systematic change in the behavior of the curves for different hydrogen isotopes, we can use the calculated data obtained by us.

As can be seen from Fig. 1, the results obtained for the spherical potential barrier are better aligned with the available experimental data. The use of a planar potential barrier leads to a decrease in the atomization coefficient

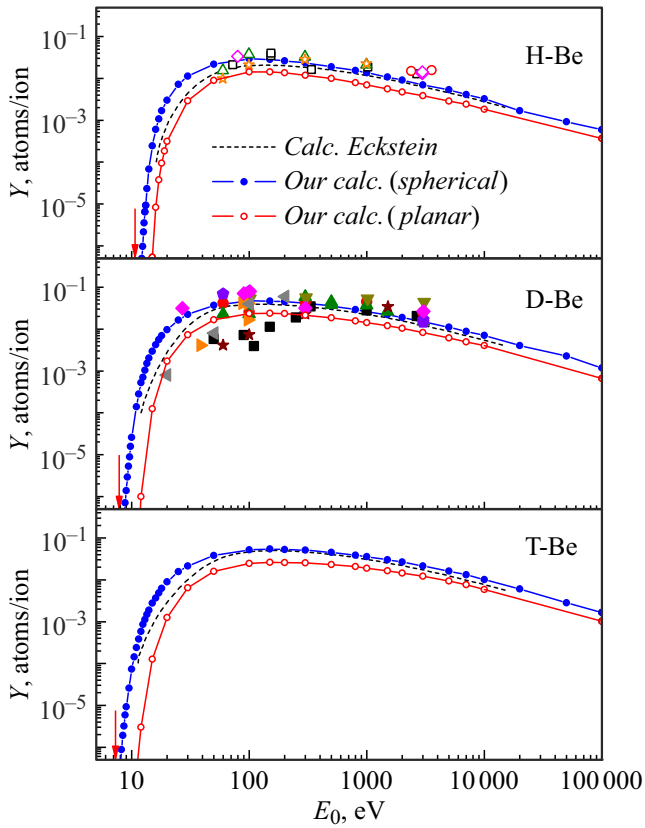

Figure 1. The relationship of the beryllium sputtering coefficient on the collision energy at the normal incidence of the beam on the target for various isotopes. Our calculation for a spherical barrier — lines with solid circles, lines with open circles — calculation for a planar barrier. Points — experimental data of various authors from the monograph [4]. Dashed line — calculation of the Eckstein group by the program SDTrimSP [5]. The arrows show the position of the spray thresholds obtained using the formula (4).

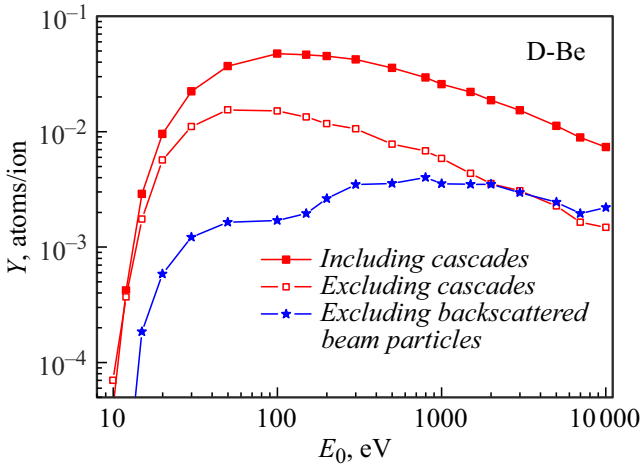

Figure 2. The two upper curves demonstrate the dispersion coefficient with and without taking into account the contribution of cascades. The curve marked with asterisks — contribution to the sputtering by the beam particles flying deep into the solid, i.e., without taking into account the contribution of the backscattered particles of the primary beam.

and a shift in the atomization threshold. A large spread of experimental data may be associated with different surface conditions in the subject experiments. In our calculations, we used both forms of the potential barrier to characterize the relationship of the sputtering coefficient on the shape of the surface.

Traditional models of sputtering are inapplicable in the considered case of bombardment of a target by light particles. The values provided by the Sigmund model [31] are five times higher than the experimental ones. In the case under consideration, the sputtering of surface layers by a flow of backscattered particles prevails.

Let us consider in more detail the model of target sputtering by light beam particles (hydrogen, deuterium and tritium). Figure 2 shows the values of the sputtering coefficient in the case of cascades formed by recoil particles, and without cascades. It can be seen that the contribution of cascades is very significant and its role increases with an increase in the initial energy. In the same figure, asterisks represent the contribution to the sputtering of recoil particles formed by beam particles moving deep into the target. As a rule, their contribution is small, and even at high energies does not exceed 12–20%. Thus, the main contribution to sputtering is made by the backscattered particles of the beam.

Fig. 3, *a* shows the relationship of the number of sprayed particles on the depth of formation of sprayed particles. It can be seen that the contribution to sputtering is mainly made by particles of the first two surface layers, and the contribution of the surface monolayer dominates.

Figure 3, *b* shows the relationship of the average depth of formation of atomized particles for various isotopes. There is a grouping of curves for different hydrogen isotopes and

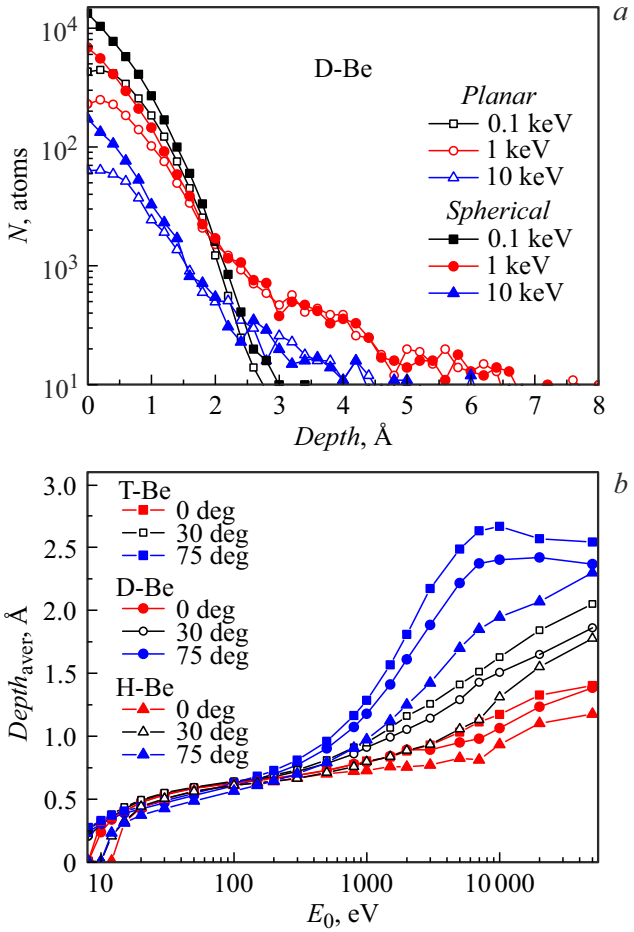

Figure 3. *a* — relationship of the number of sprayed particles on the depth of formation of the recoil particle at normal beam incidence on the target at different initial energies. Data are given for a spherical barrier (solid points) and for a planar barrier (open points). *b* — relationship of the average depth of formation of the atomized particle on the initial energy at different angles of incidence of the beam on the target. The data for the spherical barrier are given.

different angles of incidence of the beam on the target at energies less than 300 eV. With an increase in the initial energy and an increase in the angle of incidence of the beam on the target, the average depth of formation of sprayed particles increases. Nevertheless, for all energies, the average depth is less than 3 Å, which confirms our ideas that there is sputtering of near-surface layers by a flow of backscattered particles.

Consider the threshold values of energy when the sputtering coefficients tend to zero. As already mentioned, the energy transferred to the surface atom $Q = \{4M_1M_2/(M_1+M_2)^2\} \cdot E_1 > E_s$, i.e., should exceed the surface binding energy E_s, here M_1, M_2 — the masses of the incoming particle and the target atom, E_1 — average energy of backscattered particles.

The energy of a particle after a single scattering by an angle θ in the laboratory coordinate system is described by

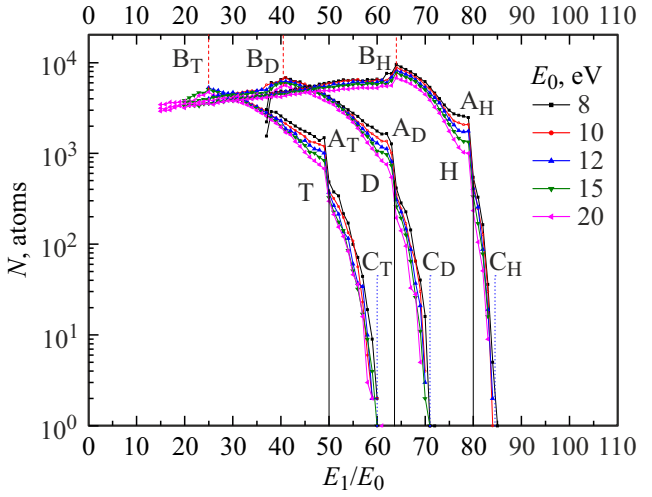

Figure 4. The relationship of the number of backscattered particles with different initial energies on the ratio of the energy of the backscattered particle to the initial energy. Curves for the scattering of three isotopes on beryllium are given. There is a sharp decline in the scattering of isotopes at the angles 90° (lines A) and 180° (lines B) at the energy corresponding to single scattering, and the high-energy component associated with multiple scattering (lines C). The lines A, B, C (see text) are marked with letters indicating the corresponding isotope $A_{H,D,T}$; $B_{H,D,T}$; $C_{H,D,T}$.

the expression:

$$\frac{E_1}{E_0} = \left(\frac{M_1}{M_1+M_2}\right)^2 \left[\cos\theta \pm \left[\left(\frac{M_2}{M_2}\right)^2 - \sin^2\theta\right]^{0.5}\right]^2. \quad (3)$$

Figure 4 shows the energy spectra of backscattered particles at small initial energies 8–20 eV. For the beam particle to fly towards the surface, it should scatter on the target atom in the laboratory coordinate system by at least 90° and its maximum energy will be $(M_2 - M_1)/(M_1 + M_2) \cdot E_0$, where E_0 is the initial energy. These positions for various isotopes are marked by lines with the index *A* in Fig. 4. The minimum particle energies will be at a single scattering by the angle 180° — lines with the index B in Fig. 4. As can be seen from Fig. 4, at the energies marked with lines, there are intensity surges in the spectrum of backscattered particles at initial energies in the threshold region. This suggests that in the case under consideration, the role of single collisions is very noticeable.

When multiple scattering is taken into account, the ratio $\xi = E_1/E_0$ increases and amounts to 0.845 for system H–Be, 0.71 for D–Be and 0.60 for system T–Be (lines with index C in Fig. 4). Multiple scattering increases the maximum possible value of the energy of the backscattered particle and the ratio ξ. Taking into account the obtained values ξ, we obtain the expression

$$E_{th} = E_s \frac{(M_1+M_2)^2}{4M_1M_2\xi}. \quad (4)$$

for the threshold energy For the systems H–Be, D–Be and T–Be we obtain the values 10.91, 7.85 and 7.37 eV, respectively. It can be seen from Fig. 1 that the results of calculation by formula (4) agree with the results of computer modeling.

3. Relationship of the sputtering coefficient and the angle of incidence of the beam on the target

Figure 5 shows the relationships of the sputtering coefficient for the systems H–Be, D–Be and T–Be and the angle of incidence θ of the beam on the target, normalized by the coefficient value for angle of incidence $\theta = 0°$ for two types of barrier. The angle is measured from the normal to the surface. This presentation reduces the overlap of curves for different initial energies and is convenient for analysis. It can be seen from Fig. 5 that the curves for different isotopes behave similarly. The sputtering coefficients increase greatly with the increase of the angle of incidence. This growth is associated with an increase in the length of the beam trajectory in the collection area of sputtered particles. The length of the trajectory increases as $1/\cos\theta$ when the

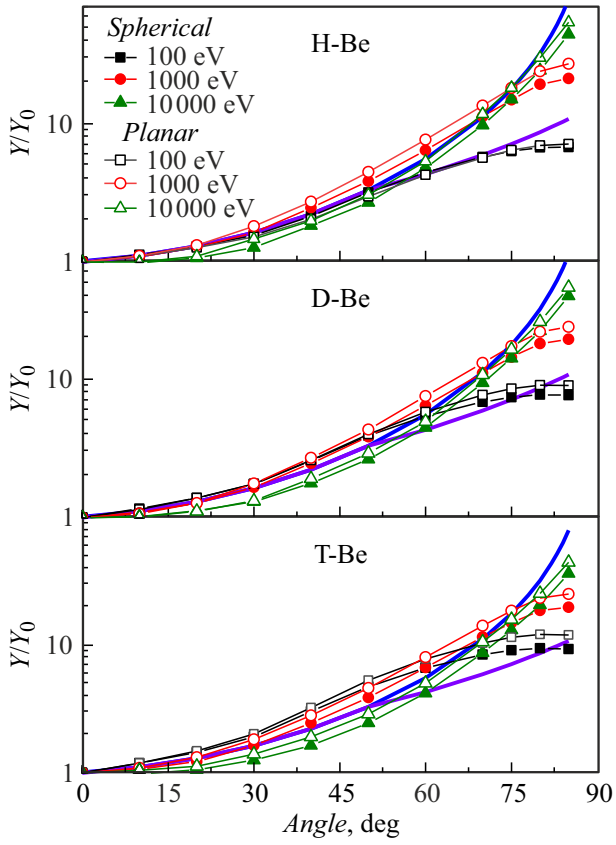

Figure 5. Angular relationships of the beryllium sputtering coefficient for three hydrogen isotopes for energies 100, 1000, 10000 eV. Lines with open symbols — calculation for a planar barrier, with solid symbols — for a spherical barrier. Solid bold lines show the theoretical limits for angular distributions.

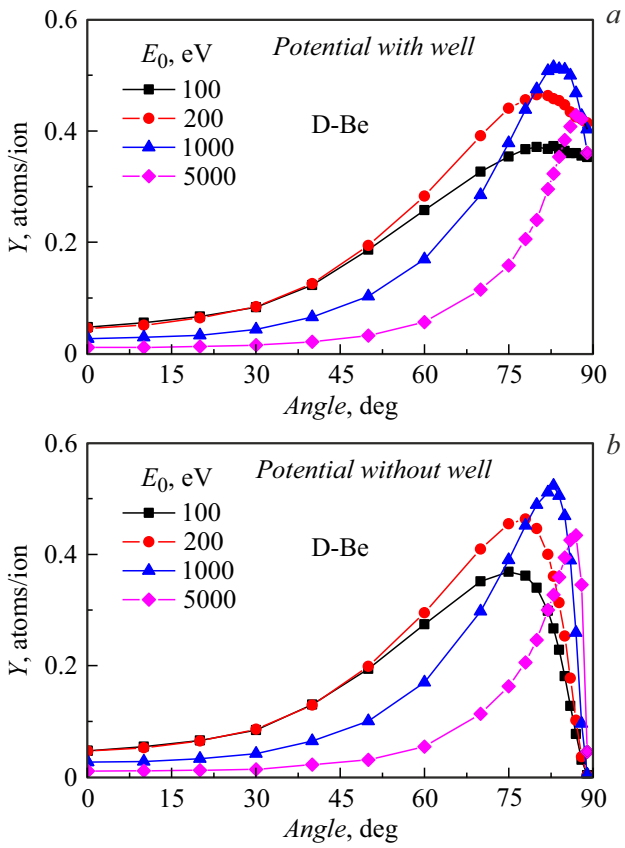

Figure 6. The relationship of the sputtering coefficient for the four primary beam energies on the angle of incidence of the beam on the target in the presence of a pit in the potential (a) and at a purely repulsive potential without a pit (b) for the system D–Be.

angle of incidence of the beam on the target changes, but is limited by the beam path in the target. The second factor that can influence the relationship of the sputtering coefficient on the angle of incidence is the difference in the scattering cross section depending on the angle of rotation of the velocity pulse for backscattered particles. In the approximation, when the contribution of backscattered particles prevails in the sputtering, it is possible to expect the relationship

$$\frac{Y(\theta)}{Y(0)} = \frac{1}{\cos\theta}\frac{\sigma(\theta_1 - \theta)}{\sigma(\theta_1)}. \qquad (5)$$

Here $\sigma(\theta)$ is differential scattering cross section by angle θ, θ_1 is the average scattering angle of the flow of backscattered particles. It can be seen from Fig. 5 that the proposed simple relationship is verified by calculated curves. The upper and lower theoretical curves set the limits of yield variation; the lower curve is plotted with account for the range of particles with an energy of 100 eV in matter.

The difference between the curves for the two types of barriers is shown in Fig. 5. When presenting data in normalized form, the difference is about 20%.

Figure 6 shows the angular relationship of the sputtering coefficient for different energies of the primary beam. The calculation was performed using the interatomic interaction potential with and without a pit. It can be seen from Fig. 6 that in the case of a purely repulsive potential (without a pit), the sputtering coefficient tends to zero at angles of incidence close to 90°. This behavior is related to the blocking effect.

In the presence of a potential pit, the blocking effect disappears and at angles of incidence close to 90°, the sputtering coefficient does not change much.

4. Energy spectra of atomized particles

The energy spectra of the sputtered particles were calculated using our program. Fig. 7, *a* shows the spectra for the system D−Be and the energies of bombarding particles in the range 100−10 000 eV. The energy spectrum drops sharply with the increase of the energy of the atomized particle E_{sp}. The spectrum broadens with the increase of the energy of the bombarding particles.

Figure 7, *b* shows the relationship of the average energy of the atomized particles on the initial energy of the bombarding particles for different angles of incidence of the beam on the target and various isotopes. At small angles of incidence of the beam on the target and collision energies less than 1000 eV, the average energy of the atomized particles increases proportionally to the energy of the bombarding particles and the relationship is the same for different isotopes. The dependence on the mass of the isotope is manifested with an increase of the angle of incidence of the beam on the target and an increase of the energy but the grouping of curves for different isotopes remains.

For the case of a surface barrier, the average energy of atomized particles increases (Fig. 7, *c*) due to a more stringent criterion for the selection of atomized particles.

5. Angular distributions of sprayed particles

Figure 8, *a* shows the distribution of sputtered particles by the angle of departure at different initial energies of bombarding particles for a spherical barrier. Calculation for the system D−Be. The number of ejected particles is given, integrated by azimuthal angle and by departure angle in the range ±2.5°. Fig. 8, *a* shows that the angular distribution has a maximum for angles ∼ 35−40°. Similar dependencies take place for other isotopes.

Fig. 8, *b* shows the same data as in Fig. 8, *a*, normalized to the maximum intensity. The relationship of the departure of sputtered particles on the angle of departure is universal. In our opinion, this is due to the multiplicity of collisions of the ejected particles.

Fig. 8, *c* shows the relationship for different isotopes. The universal relationship is preserved for a spherical barrier

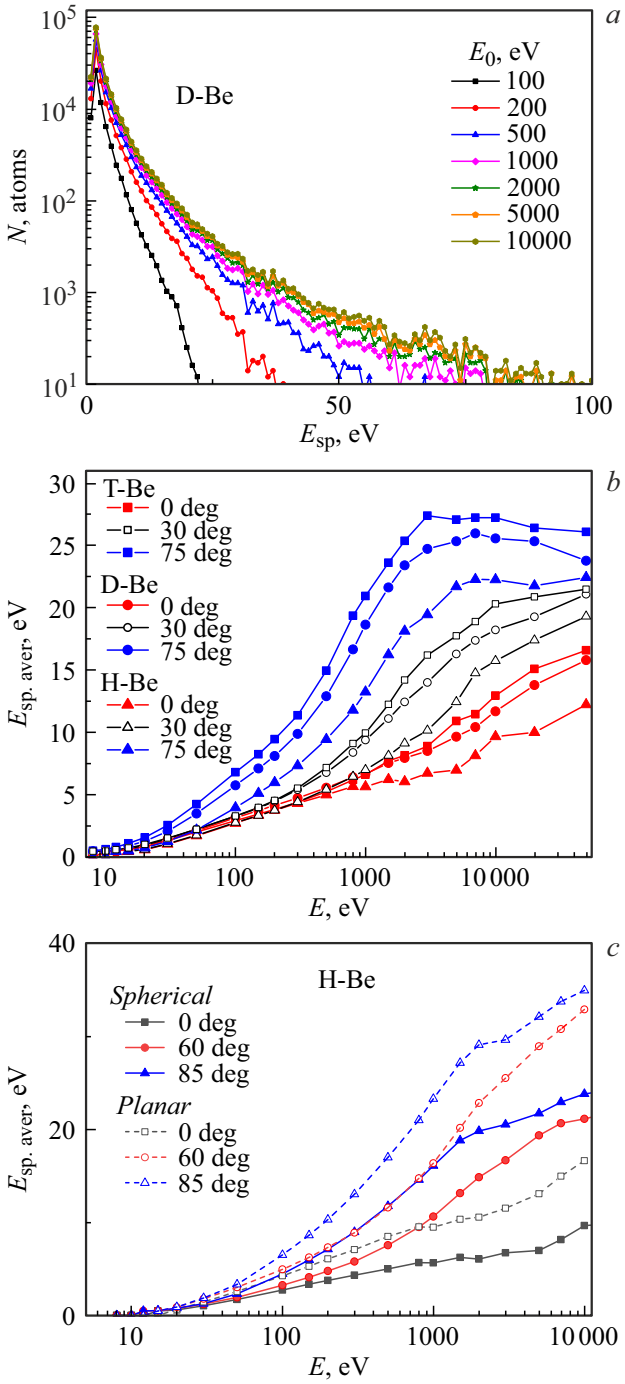

Figure 7. *a* — energy spectra of atomized particles for different atomic energies of the bombarding beam. Calculation for the system D−Be. *b* — relationship of the average energy of the atomized particle on the initial energy of the beam particles at different angles of incidence of the beam on the target. Data for three isotopes of hydrogen H, D, T and spherical barrier are given. *c* — relationship of the average energy of the atomized particle on the initial energy of the beam particles at different angles of incidence of the beam on the target. The calculation is given for the system H−Be and two types of surface barrier — spherical (spherical) and planar (planar).

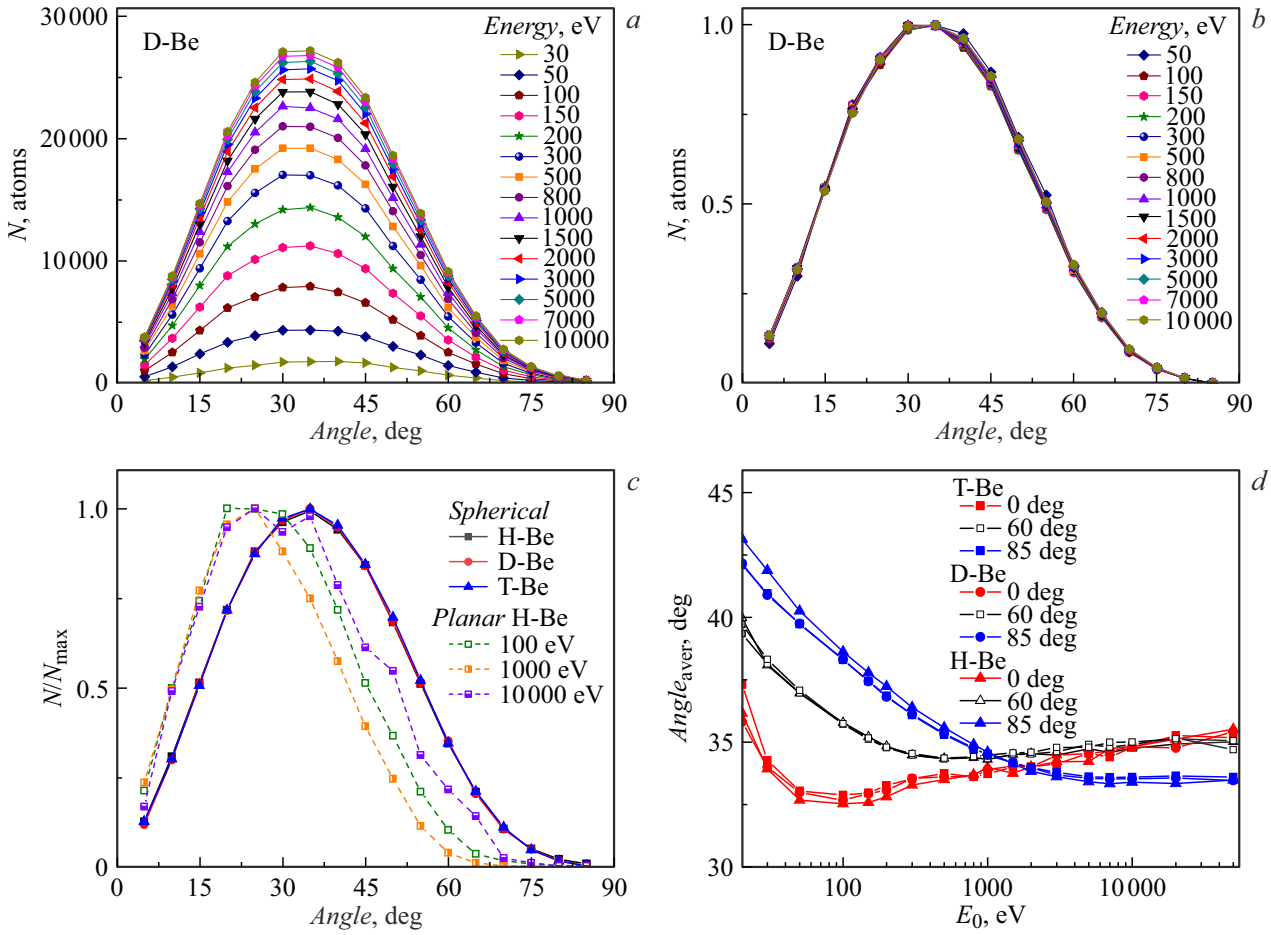

Figure 8. *a* — distribution of sprayed particles by the angle of departure at different initial energies of bombarding particles for a spherical barrier. Calculation for the system D−Be. The number of ejected particles is provided, integrated by azimuthal angle and by departure angle in the range ±2.5°. *b* — the data in Fig. 8, *a* are normalized to the maximum intensity. The normalized relationship of the intensity of the flow of sputtered particles on the angle of departure is universal. *c* — the same relationship is given for different isotopes. The universal relationship is preserved for various isotopes for a spherical barrier. For a planar barrier, there is a shift in the angular relationship. *d* — relationship of the average angle of departure of the atomized particles on the beam energy for different angles of incidence of the beam on the target and various isotopes.

and various isotopes. For a flat potential barrier, the universal relationship disappears and there is a shift of the average departure angle towards smaller angles, while with increasing energy, the magnitude of the shift decreases. Both phenomena are related to the selection criterion of the ejected particles.

We calculated the relationship of the average angle of departure on the energy of the bombarding particles (Fig. 8, *d*) to identify the difference in the angular distribution of the departure of the sprayed particles for different isotopes and the angles of incidence of the beam on the target. Fig. 8, *d* shows that practically there is no isotopic relationship of the average departure angle, while the average departure angle is maximal for low energies. The average departure angle is almost the same when the beam falls at an angle of 0° and 60° with high energies. The average angle of departure of the sputtered particles is noticeably smaller for the angle of incidence 85°.

Conclusion

The results of modeling the sputtering coefficients of polycrystalline beryllium with hydrogen isotopes in the range of collision energies 8 eV−100 keV and their dependencies on the angle of incidence of the beam on the surface, necessary for estimating the sputtering of the first beryllium wall in a tokamak ITER, are presented.

The strong influence of the surface shape on the results obtained is shown. The limiting cases of a flat potential barrier (a smooth surface) and a spherical potential barrier (a surface consisting of points) are considered. In our opinion, the strong variation in the available experimental data is due to the difference in the state of the surface, especially when the surface is bombarded with an intense ion beam. Beams with high intensity are used for measuring the sputtering coefficients by the weight method.

The impact of cascades of collisions on the sputtering coefficient is modeled. The dependences of the average depth of formation of the atomized particle on the energy of the bombarding particles at different angles of incidence of the beam on the target are obtained. The energy spectra and angular dependences of the departure of the atomized particles for different atomic energies of the bombarding beam are calculated. This information is important for assessing the entry of particles into the plasma.

It is shown that the presence of a potential pit in the system of an incident particle−surface changes the nature of the dependence of the sputtering coefficient on the angle of incidence at small sliding angles.

In our work [32], for typical parameters of the ITER tokamak, a simulation of the sputtering of a beryllium wall by streams of fast deuterium and tritium atoms leaving the plasma was carried out. The resulting value of the receipt of atomized Be atoms was $6.5 \cdot 10^{17}$ atoms/s per square meter of the wall. With typical parameters of ion retention in plasma, this will be 2.5−4.2% of the concentration of ions in plasma. Such a significant content of Be ions in the separatrix area can lead to an increase in the sputtering of the divertor from W by multicharged Be ions.

The detailed data obtained in this work on the sputtering coefficients and dependences on the angle of incidence of the beam particles on the target, as well as on the energy and angular dependences of the departure of the sprayed particles provide a reliable basis for estimating the intake of beryllium admixture into the plasma.

Conflict of interest

The authors declare that they have no conflict of interest.

References

[1] K. Schmid. Nucl. Fusion, **48** (10), 105004 (2008). DOI: 10.1088/0029-5515/48/10/105004

[2] A.S. Kukushkin, H.D. Pacher, V. Kotov, G.W. Pacher, D. Reiter. Fusion Eng. Des., **86** (12), 2865 (2011). DOI: 10.1016/j.fusengdes.2011.06.009

[3] P.Yu. Babenko, M.I. Mironov, V.S. Mikhailov, A.N. Zinoviev. Plasma Phys. Control. Fusion, **62** (4), 045020 (2020). DOI: 10.1088/1361-6587/ab7943

[4] R. Behrisch, W. Eckstein. *Sputtering by Particle Bombardment* (Springer, Berlin, 2007), DOI: 10.1007/978-3-540-44502-9

[5] R.E.H. Clark. *Atomic and Plasma-Material Interaction Data for Fusion* (IAEA, Vienna, 2001), v. 7, Part B.

[6] W.D. Wilson, L.G. Haggmark, J.P. Biersack. Phys. Rev. B, **15** (5), 2458 (1977). DOI: 10.1103/PhysRevB.15.2458

[7] E. Salonen, K. Nordlund, J. Keinonen, C.H. Wu. J. Nucl. Mater., **313**−**316**, 404 (2003). DOI: 10.1016/S0022-3115(02)01397-1

[8] K. Nordlund, C. Björkas, K. Vörtler, A. Meinander, A. Lasa, M. Mehine, A.V. Krasheninnikov. Nucl. Instr. Meth. B, **269** (11), 1257 (2011). DOI: 10.1016/j.nimb.2010.12.080

[9] M.I. Airila, C. Björkas, A. Lasa, A. Meinander, K. Nordlund, K. Vörtler. J. Nucl. Mater., **438**, S589 (2013). DOI: 10.1016/j.jnucmat.2013.01.123

[10] X. Yang, A. Hassanein. Appl. Surf. Sci., **293**, 187 (2014). DOI: 10.1016/j.apsusc.2013.12.129

[11] D.S. Meluzova, P.Yu. Babenko, A.N. Zinoviev, A.P. Shergin. Pisma v ZhTF,**46** (24), 19 (2020) (in Russian). DOI: 10.21883/PJTF.2020.24.50422.18487

[12] A. Lopez-Cazalilla, J. Jussila, K. Nordlund, F. Granberg. Comput. Mater. Sci., **216**, 111876 (2023). DOI: 10.1016/j.commatsci.2022.111876

[13] C. Björkas, K. Nordlund, S. Dudarev. Nucl. Instr. Meth. B, **267** (18), 3204 (2009). DOI: 10.1016/j.nimb.2009.06.123

[14] X.-C. Li, X. Shu, Y.-N. Liu, Y. Yua, F. Gao, G.-H. Lu. J. Nucl. Mater., **426** (1−3), 31 (2012). DOI: 10.1016/j.jnucmat.2012.03.039

[15] M.-C. Marinica, L. Ventelon, M.R. Gilbert, L. Proville, S.L. Dudarev, J. Marian, G. Bencteux, F. Willaime. J. Phys. Condens. Matter., **25**, 395502 (2013). DOI: 10.1088/0953-8984/25/39/395502

[16] A.E. Sand, J. Dequeker, C.S. Becquart, C. Domain, K. Nordlund. J. Nucl. Mater., **470**, 119 (2016). DOI: 10.1016/j.jnucmat.2015.12.012

[17] P.Yu. Babenko, V.S. Mikhailov, A.N. Zinoviev. Pisma v ZhTF (2023) (in Russian).

[18] W. Eckstein, *Computer Simulation of Ion–Solid Interactions* (Springer, 1991).

[19] P.Yu. Babenko, A.N. Zinoviev, V.S. Mikhailov, D.S. Tensin, A.P. Shergin, Pisma v ZhTF, **48**, 10 (2022). (in Russian). DOI: 10.21883/PJTF.2022.14.52862.19231

[20] D.S. Meluzova, P.Yu. Babenko, A.P. Shergin, K. Nordlund, A.N. Zinoviev. Nucl. Instr. Meth. B, **460**, 4 (2019). DOI: 10.1016/j.nimb.2019.03.037

[21] P.Yu. Babenko, A.N. Zinoviev, D.S. Tensin. ZhTF, **92** (11), 1643 (2022) (in Russian). DOI: 10.21883/JTF.2022.11.53436.151-22

[22] A.N. Zinoviev, P.Yu. Babenko, K. Nordlund. Nucl. Instr. Meth. B, **508**, 10 (2021). DOI: 10.1016/j.nimb.2021.10.001

[23] A.N. Zinoviev, K. Nordlund. Nucl. Instr. Meth. B, **406**, 511 (2017). DOI: 10.1016/j.nimb.2017.03.047

[24] C. Bjorkas, N. Juslin, H. Timko, K. Vortler, K. Nordlund, K. Henriksson, P. Erhart. J. Phys.: Condens. Matter., **21**, 445002 (2009). DOI: 10.1088/0953-8984/21/44/445002

[25] M.V. Prokof'ev, V.V. Svetukhin, M.Yu. Tikhonchev. Izv. of the Samara NTs RAN, **15**, 1024 (2013) (in Russian).

[26] B.P. Nikol'skii, *Spravochnik khimika* (Khimiya, L., 1966) (in Russian).

[27] Y.R. Luo. *Comprehensive Handbook of Chemical Bond Energies* (CRC Press, Boca Raton, 2007)

[28] D. Primetzhofer, S. Rund, D. Roth, D. Goebl, P. Bauer. Phys. Rev. Lett., **107**, 163201 (2011). DOI: 10.1103/PhysRevLett.107.163201

[29] A. Mann, W. Brandt. Phys. Rev. B, **24**, 4999 (1981). DOI: 10.1103/PhysRevB.24.4999

[30] J.F. Ziegler, J.P. Biersack. SRIM. http://www.srim.org

[31] P. Sigmund. Phys. Rev., **184**, 383 (1969). DOI: 10.1103/PhysRev.184.383

[32] P.Yu. Babenko, M.I. Mironov, V.S. Mikhailov, A.N. Zinoviev. Plasma Phys. Control. Fusion, **62**, 045020 (2020). DOI: 10.1088/1361-6587/ab7943

Translated by A.Akhtyamov